COMMUNICATION

Solid-state behaviors of imines: Colossal biaxial positive thermal expansion, motion capability, and phase transitions

Navkiran Juneja, Ethan Zahid, Daniel K. Unruh and Kristin M. Hutchins*

Received 00th January 20xx,
Accepted 00th January 20xx

DOI: 10.1039/x0xx00000x

Pedal motion or static disorder in single-component solids containing imine groups is demonstrated. Unique solid-state behaviors including colossal biaxial positive thermal expansion in one solid and a temperature-dependent phase transition in another are discussed. Imines exhibit torsional flexibility, which differs from the isoelctronic azo and olefin groups and influences solid-state behaviors.

Solid-state materials that exhibit dynamic behaviors are rapidly gaining interest for use in molecular machines,[1] switches,[2] and rotors.[3] Molecules exhibiting structures similar to that of azobenzenes, *E*-stilbenes, and *N*-Benzylideneanilines (Fig. 1a) are known to undergo *cis-trans* isomerizations, which give rise to changes in optical and mechanical (e.g. bending) behaviors.[4] In addition to isomerization, molecules with these functional groups can also undergo dynamic pedal motion in the solid state (Fig. 1b). This molecular motion occurs as a result of interconversion between conformers and is analogous to bicycle pedals and the crank arm attached to them.[5, 6] The solid-state motion is observed via disorder, and the percent occupancies of each conformer can be quantified as a function of temperature using variable temperature single-crystal X-ray diffraction (VT-SCXRD).

Pedal motion has been studied most frequently in azobenzene- and stilbene-type molecules,[6] while pedal motion in imine-based solids has been studied to a much lesser extent.[7] For example, *N*-benzylideneaniline, which is isoelectronic to azobenzene and *E*-stilbene (Fig. 1a), exhibits static disorder in the crystalline state, wherein there is no interconversion between conformers.[8] A few functionalized derivatives of *N*-benzylideneaniline (e.g. 4-nitro, 4-chloro, 4-methyl) have been shown to exhibit pedal motion.[9] *Trans*-stilbenes or *trans*-azobenzenes typically crystallize in nearly planar geometries. On the other hand, *trans*-*N*-benzylideneaniline crystallizes in a non-planar geometry with the aniline ring twisted out of the plane with the bridge (C-N=C-C moiety) by 40-55°.[8, 10] The torsional flexibility of the imine group impacts crystal packing and, ultimately, could influence solid-state properties. Additionally, imine-based linkages are frequently used in covalent-organic and metal-organic frameworks[11, 12] and the dynamic capability of the group could influence these classes of materials as well.

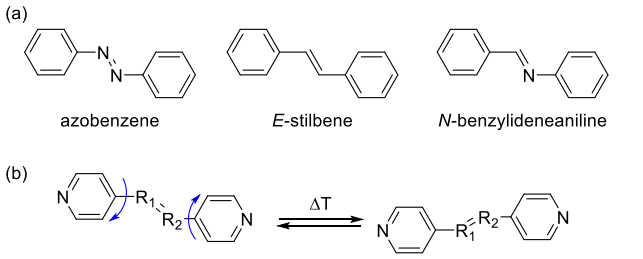

Fig. 1. (a) Chemical structures of motion-capable molecules and (b) bipyridine molecule undergoing pedal motion.

Our group has previously investigated the symmetrical bipyridine molecules 4,4'-azopyridine (4,4'-AP) and 1,2-di(4-pyridyl)ethylene (4,4'-BPE), which include an azo or olefin group, respectively. 4,4'-AP and 4,4'-BPE do not exhibit pedal motion as single-component solids,[13] but the motion capability can be unlocked in multi-component solids (e.g. cocrystals, metal-organic complexes).[14] Importantly, we demonstrated solids containing 4,4'-AP and 4,4'-BPE that undergo dynamic pedal motion also exhibit large thermal expansion along the motion direction.[15] Thermal expansion (TE) is the tendency of matter to undergo a change in size in response to temperature alterations. TE of solid materials is strongly dependent on the chemical composition and the interactions that sustain it.[16] Most materials expand upon heating, which is called positive thermal expansion (PTE), while some materials contract upon heating, exhibiting negative thermal expansion (NTE).[17] The

Department of Chemistry and Biochemistry, Texas Tech University, 1204 Boston Avenue, Lubbock, Texas 79409, USA. Email: kristin.hutchins@ttu.edu

†Electronic Supplementary Information (ESI) available: Experimental details, X-ray diffraction data, thermal data, thermal expansion analysis. CCDC 2072411-2072416, 2072254-2072263, and 2072417-2072428. For ESI and crystallographic data see DOI: 10.1039/x0xx00000x

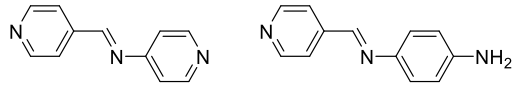

BPI **PI-NH$_2$**

Fig. 2. Structures of pyridines functionalized with motion-capable imines studied in this work.

term colossal has been designated to identify systems that exhibit TE coefficients greater than or equal to 100 MK^{-1}.[18]

We, thus, sought to investigate pedal motion ability and impacts on TE behavior for pyridine-based compounds containing imine groups (Fig. 2). Here, we show *N*-(4-pyridinylmethylene)-4-pyridinamine (**BPI**), which is isoelectronic with 4,4'-AP and 4,4'-BPE, exhibits static disorder as a single-component solid. **BPI** also exhibits colossal biaxial PTE, arising from a combination of torsional flexibility, solid-state packing, and weak intermolecular forces. We also demonstrate the unique solid-state behavior of imines in a related molecule, (*E*)-4-((pyridin-4-ylmethylene)amino)aniline (**PI-NH$_2$**), wherein the compound undergoes pedal motion and the imine bond flips orientation as a function of temperature. The torsional flexibility of the imine impacts crystal packing, solid-state motion, and TE in a way that differs from the isoelectronic azo and olefin derivatives.

BPI was synthesized using a literature procedure (see ESI). **PI-NH$_2$** was synthesized by grinding benzene-1,4-diamine and 4-pyridine carboxaldehyde in 1:1 ratio with 100 µL of methanol for a period of 15-20 minutes using a mortar and pestle. Single crystals suitable for SCXRD studies were grown by dissolving 10-15 mg of each compound in a minimal amount of an appropriate solvent (hexanes for **BPI** and acetonitrile for **PI-NH$_2$**) and allowing the solution to evaporate slowly over a couple of days. VT SCXRD experiments were performed by collecting data over the temperature range of 290-190 K at 20 K intervals (Tables S1-S9, Fig. S7-S10). The TE coefficients along with the principal axes (X_1, X_2, and X_3) were calculated using the software, PASCal.[19]

Although **BPI** is a structurally simple molecule, its crystal structure has not been reported until now.[20] **BPI** crystallizes in the monoclinic space group, *C2/m*. The asymmetric unit contains one and a half pyridine rings and the imine. The pyridine rings are twisted from planarity by 90°, and the molecule is disordered at room temperature. VT SCXRD data demonstrated that **BPI** exhibits static disorder as confirmed by nearly no change in the site occupancies as a function of temperature (Table 1). While **BPI** exhibits static disorder and the rings lie twisted, the analogous azo- and olefin-functionalized compounds (4,4'-AP and 4,4'-BPE) do not exhibit disorder as single components and the rings lie coplanar.[13]

Along the crystallographic *b* axis, adjacent molecules interact via C-H(α)···N(pyr) hydrogen bonds (3.638 Å) forming a zig-zag pattern (Fig. 3a). The pyridine rings involved in these hydrogen bonds are crystallographically identical (N1) and lie twisted from the imine and other pyridine ring. The second pyridine ring (N3), which lies in the same plane as the imine, has nearest contact with the beta hydrogens on the pyridine rings lying above and below it. In these hydrogen bonds, the hydrogen atoms do not lie in the plane of the aromatic ring where the lone pair on the nitrogen would be, but the C-H-N angles are within accepted limits. The C-H···N contacts facilitate formation of a sheet-like structure that extends in the *ab* plane. In the sheet, the imine groups and one pyridine ring on each molecule are stacked in a face-to-face arrangement. Neighboring sheets interact via weak C-H(imine)···N(pyr), C-H(β)···N(pyr), and C-H(β)···π interactions (Fig. 3b).

Table 1. Major site occupancies for **BPI** as a function of temperature. The error is denoted in parenthesis.

Temperature (K)	Site occupancy (major conformation)
290	0.505(7)
270	0.507(7)
250	0.510(6)
230	0.512(6)
210	0.506(5)
190	0.495(11)

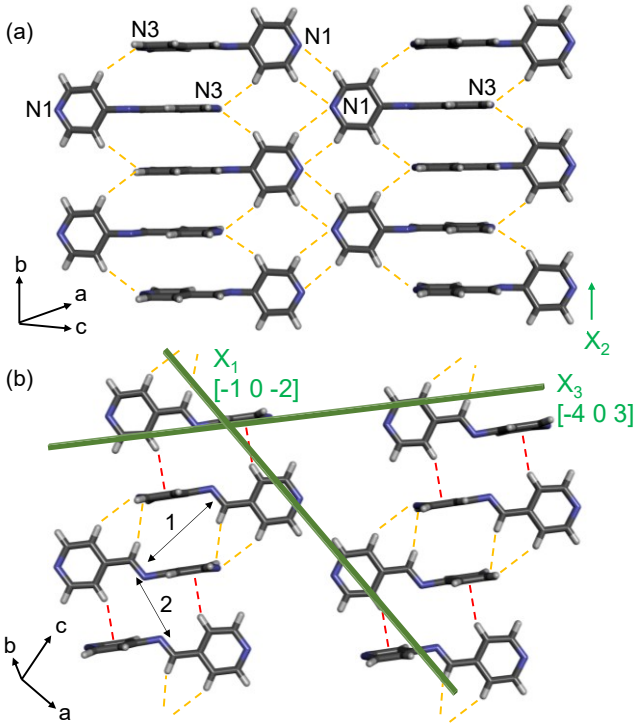

Fig. 3. X-ray crystal structures of **BPI** at 290 K: (a) crystal packing along the *b* axis highlighting principal axis X_2 and (b) packing of sheets highlighting principal axes X_1 and X_3. Disorder has been omitted for clarity. Hydrogen bonds are shown with yellow dashed lines. The C-H(β)···π interactions are shown with red dashed lines. The distance between molecules in neighboring sheets is shown with black double-headed arrows. There are two different separations, labeled 1 and 2.

Upon cooling **BPI** to 190 K, the distance between molecules in neighboring sheets increases by 0.094 Å (centroid-centroid distance, see black arrow labeled 1 in Fig. 3b). The C-H(imine)···N(pyr) and C-H(β)···N(pyr) interactions between sheets also increase by 0.032 Å and 0.081 Å, respectively (Table S11). These increases in length upon cooling afford NTE behavior along the X_1 axis (α_{X1} = -73(5) MK^{-1}). Colossal PTE is observed along the X_2 and X_3 axes (α_{X2} = 118(3) MK^{-1}; α_{X3} = 176(16) MK^{-1}). Overall, the volumetric expansion coefficient for **BPI** is also colossal (α_V = 228(14) MK^{-1}). The X_2 axis corresponds to the crystallographic *b* axis of **BPI**, which decreases by 1.2% as the crystal is cooled from 290 to 190 K (Fig. S6). The intermolecular interactions lying along the X_2 axis include the C-

H(α)···N(pyr) and C-H(β)···N(pyr) hydrogen bonds, which decrease by 0.05 and 0.04 Å upon cooling, respectively. The π···π stacking separations also decrease by ca. 0.04 Å as the temperature is lowered. The C-H(β)···π interactions are the primary intermolecular forces contributing to expansion along the X_3 axis and decrease by 0.143 Å upon cooling. The distance between molecules in neighboring sheets also decreases by 0.151 Å (centroid-centroid distance, see black arrow labeled 2 in Fig. 3b). The static disorder of **BPI** likely does not contribute significantly to the TE. While biaxial PTE alone is not novel,[21] the magnitude of the biaxial PTE for **BPI** is significant and results from weak intermolecular interactions.

To further investigate the motion capability of pyridyl imines, we synthesized **PI-NH$_2$**, wherein the second pyridine is replaced by a hydrogen-bond-donating amine group. **PI-NH$_2$** crystallized in the Sohncke space group $P2_12_12_1$. The asymmetric unit consists of one full molecule of **PI-NH$_2$**, and, unlike **BPI**, the two aromatic rings of **PI-NH$_2$** lie nearly coplanar as the angle between them is only 5°. Molecules of **PI-NH$_2$** self-assemble to form 1D hydrogen-bonded chains that extend along the crystallographic *c* axis via N-H···N(pyr) forces (Fig. 4a). Adjacent chains stack edge-to-face along the crystallographic *b* axis and are twisted at an angle of ca. 64° at 290 K (Fig. 4b). The chains interact via N-H···π and C-H···π interactions, with separations of 3.625 and 3.629 Å, respectively.

During the VT SCXRD experiment for **PI-NH$_2$**, a phase transition was observed; however, the reversibility and occurrence of the phase transition depends on the cooling method (Fig. S8-S9). SCXRD data was first collected at 290 K, and the crystal was slowly cooled down to 100 K while collecting full data sets at intervals of 20 K to quantify the site occupancies of the disordered molecule. At 290 K, the pyridine ring and imine group of **PI-NH$_2$** are disordered (Table 2). When the crystal was cooled from 290 to 270 K, a phase transition occurred as a result of the imine bond flipping its orientation (Fig. 5a). Specifically,

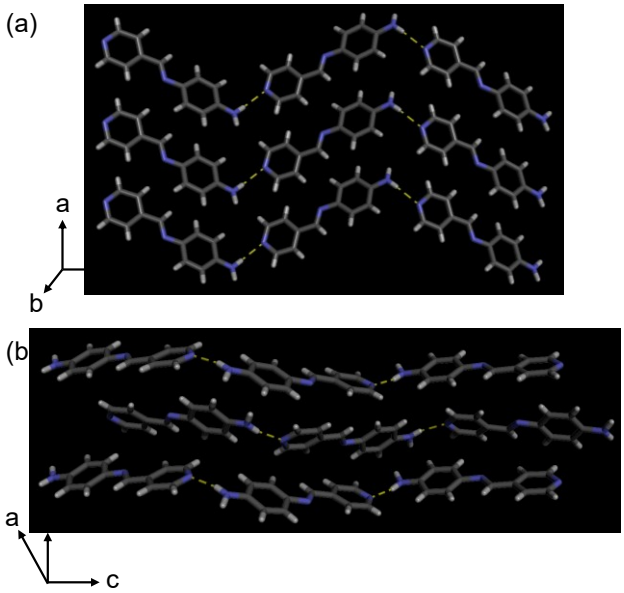

Fig. 4. X-ray crystal structures of **PI-NH$_2$** at 290 K: (a) 1D hydrogen-bonded chains and (b) edge-to-face packing of chains. Disorder has been omitted for clarity. Hydrogen bonds shown with yellow dashed lines.

the transition took place during the first 650 frames collected out of 2700 at 270 K. The data from the first 650 frames was omitted from the 270 K data set. As a result of transition, the length of the *a* axis increased by ca. 0.13 Å and the *b* and *c* axes decreased by ca. 0.11 and 0.10 Å, respectively. The volume of the unit cell increased by 3.8 Å^3 (ca. 0.4%). Upon examination of the structure, the primary intermolecular interactions still sustain the solid (N-H···N hydrogen bonds); however, the bond length shortened by 0.06 Å. Moreover, the site occupancies of **PI-NH$_2$** changed by 10% between 290 and 270 K (Table 2). Upon further cooling, **PI-NH$_2$** continued to undergo slight pedal motion from 270-230 K, only one conformer is present at 210 K, and the solid remained fully ordered until 100 K (Fig. 5a). The unit cell volume consistently decreased from 1021 Å^3 to 991 Å^3 as the crystal was slowly cooled from 270-100 K.

To further investigate the phase transition of **PI-NH$_2$**, the crystal was flash cooled to 190 K, warmed to 290 K while collecting full data sets every 20 K, then cooled back to 190 K while collecting full data sets every 20 K. When the crystal is first placed on the instrument and flash cooled to 190 K, it lies in the smaller volume cell (995 Å^3). During the warming cycle, the

Table 2. Major site occupancy and volume of the unit cell for **PI-NH$_2$** when the crystal is slowly cooled from 290 K to 100 K. Errors are shown in parenthesis.

Temperature (K)	Site occupancy (major conformation)	Unit cell volume (Å^3)
290	0.844(5)	1017.58(3)
270	0.948(4)	1021.38(14)
250	0.967(3)	1015.96(3)
230	0.976(3)	1012.12(3)
210	1.00	1008.33(2)
190	1.00	1004.47(2)
170	1.00	1001.20(2)
150	1.00	998.23(2)
130	1.00	995.39(3)
100	1.00	991.03(3)

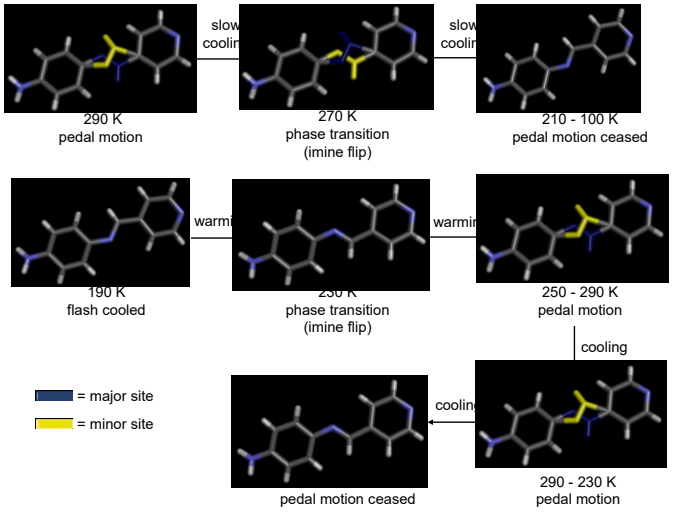

Fig. 5. (a) Disordered and ordered states of **PI-NH$_2$** when the crystal is mounted at room temperature and slowly cooled. (b) Disordered and ordered states of **PI-NH$_2$** when the crystal is flash cooled, warmed to room temperature, and slowly cooled. Disorder is only shown for the imine group for clarity. The major site of the imine is shown in dark blue, and the minor site is in yellow.

Table 3. Major site occupancy and unit cell volume for **PI-NH$_2$** during the flash cooling, heating, and cooling cycles. Errors are shown in parenthesis.

Temperature (K)	Cycle part	Site occupancy (major conformation)	Unit cell volume (Å^3)
190	flash cooled	1.00	995.58(14)
210	warming	1.00	999.34(15)
230	warming	1.00	1010.83(2)
250	warming	0.969(3)	1015.74(18)
270	warming	0.946(4)	1019.78(14)
290	warming	0.899(4)	1024.10(2)
270	cooling	0.944(4)	1019.70(19)
250	cooling	0.966(3)	1015.64(17)
230	cooling	0.976(3)	1011.78(16)
210	cooling	1.00	1008.01(14)
190	cooling	1.00	1004.30(14)

phase transition occurred at 230 K and two data sets were obtained (before and after the transition). Interestingly, during the warming cycle, the imine bond flipping occurred at a temperature 40 K lower than it did during the original slow cooling cycle (230 K following flash cooling and warming versus 270 K during slow cooling). Upon reaching a temperature of 250 K during the warming cycle, disorder was observed as **PI-NH$_2$** begins to undergo pedal motion (Table 3). After reaching 290 K, the same crystal was cooled down to 190 K (collecting full data sets every 20 K) and no phase transition was observed. During the cooling cycle, the pedal motion ceased at 210 K, identical to the original slow cooling cycle (Table 3, Fig. 5b).

Phase transitions in crystalline materials can also be characterized by differential scanning calorimetry (DSC). DSC experiments were attempted to investigate the phase transition of **PI-NH$_2$**. Since the change in the unit cell dimensions was relatively small, we did not observe any signals indicative of a phase transition during DSC experiments using a variety of cooling and heating rates (Fig. S2). The TE coefficients were not calculated for **PI-NH$_2$** due to the temperature-dependent phase transitions.

Here, we described how the torsional flexibility of imine groups influences solid-state packing in single-component solids. Biaxial colossal PTE is attained in the bipyridine compound **BPI**, and pedal motion accompanied by a phase transition/conformational change occured in **PI-NH$_2$**. This study demonstrates that the imine functional group is not only pedal-motion capable, but could unlock unique solid-state behaviors that differ from its isoelectronic olefin and azo compounds.

K.M.H. gratefully acknowledges financial support from the National Science Foundation (DMR-2045506). The authors thank Dr. Sindee Simon and Dr. Yung Koh for collecting the TGA and DSC data and Dr. Eric Reinheimer for helpful conversations.

Conflicts of interest

There are no conflicts to declare.

Notes and references

1. T. Van Leeuwen, A. S. Lubbe, P. Štacko, S. J. Wezenberg and B. L. Feringa, *Nat. Rev. Chem.*, 2017, **1**, 0096.
2. A. Goulet-Hanssens, F. Eisenreich and S. Hecht, *Adv. Mater.*, 2020, **32**, 1905966.
3. L. Catalano and P. Naumov, *CrystEngComm*, 2018, **20**, 5872-5883.
4. N. R. King, E. A. Whale, F. J. Davis, A. Gilbert and G. R. Mitchell, *J. Mater. Chem.*, 1997, **7**, 625-630; O. S. Bushuyev, T. C. Corkery, C. J. Barrett and T. Friščić, *Chem. Sci.*, 2014, **5**, 3158-3164.
5. J. Harada, K. Ogawa and S. Tomoda, *Acta Cryst.*, 1997, **B53**, 662-672; J. Harada and K. Ogawa, *J. Am. Chem. Soc.*, 2004, **126**, 3539-3544.
6. J. Harada and K. Ogawa, *J. Am. Chem. Soc.*, 2001, **123**, 10884-10888; J. Harada and K. Ogawa, *Chem. Soc. Rev.*, 2009, **38**, 2244–2252.
7. G. Kumar, M. Singh, R. Goswami and S. Neogi, *ACS Appl. Mater. Interfaces*, 2020, **12**, 48642-48653.
8. J. Harada, M. Harakawa and K. Ogawa, *Acta Cryst.*, 2004, **B60**, 578-588.
9. J. Harada, M. Harakawa and K. Ogawa, *Acta Cryst.*, 2004, **B60**, 589-597.
10. H. B. Burgi and J. D. Dunitz, *Helv. Chim. Acta* 1970, **53**, 1747-1764.
11. H. L. Nguyen, C. Gropp and O. M. Yaghi, *J. Am. Chem. Soc.*, 2020, **142**, 2771-2776.
12. X. Li, J. Wang, F. Xue, Y. Wu, H. Xu, T. Yi and Q. Li, *Angew. Chem. Int. Ed.*, 2021, **60**, 2534-2540.
13. K. M. Hutchins, K. A. Kummer, R. H. Groeneman, E. W.Reinheimer, M. A. Sinnwell, D. C. Swenson and L. R.MacGillivray, *CrystEngComm*, 2012, **00**, 1-3; J. Vansant and G. Smets, *J. Org. Chem.*, 1980, **45**, 1557-1565; L. Gao, Y. Hao, X. Zhang, X. Huang, T. Wang and H. Hao, *CrystEngComm*, 2020, **22**, 3279-3286.
14. Y.-G. Huang, Y. Shiota, S.-Q. Su, S.-Q. Wu, Z.-S. Yao, G.-L. Li, S. Kanegawa, S. Kang, T. Kamachi, K. Yoshizawa, Katsuhiko Ariga and O. Sato, *Angew. Chem. Int. Ed.*, 2016, **55**, 14628 –14632; A. V. Savchenkov, A. V. Vologzhanina, D. V. Pushkin, L. B. Serezhkina and V. N. Serezhkin, *Inorg. Chim. Acta*, 2019, **498**, 119089; A. M. Puthan, Peedikakkal and J. J. Vittal, *Chem. Eur. J.*, 2008, **14**, 5329-5334.
15. N. Juneja, D. K. Unruh, E. Bosch, R. H. Groeneman and K. M. Hutchins, *New J. Chem.*, 2019, **43**, 18433-18436; K. M. Hutchins, D. K. Unruh, F. A. Verdu and R. H. Groeneman, *Cryst. Growth Des.*, 2018, **18**, 566-570.
16. A. I. Kitaigorodsky, *Molecular Crystals and Molecules*, Academic Press, New York, 1973; J. Salud, M. Barrio, D. O. Lopez, J. L. Tamarit and X. Alcobe, *J. Appl. Cryst.*, 1998, **31**, 748-757; L. Negi, A. Shrivastava and D. Das, *Chem. Commun.*, 2018, **54**, 10675-10678.
17. G. D. Barrera, J. A. O. Bruno, T. H. KBarron and N. L. Allan, *J. Phys.: Condens. Matter*, 2005, **17**, R217–R252; A. Sanson, *Mater. Res. Lett.*, 2019, **7**, 412–417.
18. A. L. Goodwin, M. Calleja, M. J. Conterio, M. T. Dove, J. S. O. Evans, D. A. Keen, L. Peters and M. G. Tucker, *Science*, 2008, **319**, 794-797.
19. M. J. Cliffe and A. L. Goodwin, *J. Appl. Cryst.*, 2012, **45**, 1321–1329
20. CSD ver. 5.41 Cambridge Structural Database, November 2019 + 3 updates.
21. D. Das and L. J. Barbour, *CrystEngComm*, 2018, **20**, 5123-5126; E. R. Engel, V. J. Smith, C. X. Bezuidenhout and L. J. Barbour, *Chem. Mater.*, 2016, **28**, 5073-5079.

